Journal of Computational Physics 476 (2023) 111907

Contents lists available at ScienceDirect

Journal of Computational Physics

journal homepage: www.elsevier.com/locate/jcp

Boundary and interface methods for energy stable finite difference discretizations of the dynamic beam equation

Gustav Eriksson *, Jonatan Werpers, David Niemelä, Niklas Wik, Valter Zethrin, Ken Mattsson

Department of Information Technology, Uppsala University, PO Box 337, S-751 05 Uppsala, Sweden

ARTICLE INFO

Article history:
Received 26 July 2021
Received in revised form 11 October 2022
Accepted 1 January 2023
Available online 6 January 2023

Keywords:
Dynamic beam equation
Boundary treatment
Summation by parts
Finite differences
High order methods

ABSTRACT

We consider energy stable summation by parts finite difference methods (SBP-FD) for the homogeneous and piecewise homogeneous dynamic beam equation (DBE). Previously the constant coefficient problem has been solved with SBP-FD together with penalty terms (SBP-SAT) to impose boundary conditions. In this work, we revisit this problem and compare SBP-SAT to the projection method (SBP-P). We also consider the DBE with discontinuous coefficients and present novel SBP-SAT, SBP-P, and hybrid SBP-SAT-P discretizations for imposing interface conditions. To demonstrate the methodology for two-dimensional problems, we also present a discretization of the piecewise homogeneous dynamic Kirchoff-Love plate equation based on the hybrid SBP-SAT-P method. Numerical experiments show that all methods considered are similar in terms of accuracy, but that SBP-P can be more computationally efficient (less restrictive time step requirement for explicit time integration methods) for both the constant and piecewise constant coefficient problems.

1. Introduction

The dynamic beam equation (DBE) is a standard beam theory model describing the motion of free vibrations of an Euler-Bernoulli beam. The derivation of the equation dates back to the 18th century but it is still used in engineering applications today. For example, in the construction of infrastructure involving beams such as buildings, bridges, and railways.

Most of the literature on the DBE focus on solving the constant coefficient problem in the frequency domain. By taking the Laplace transform of the equation one can, for specific boundary conditions and external loads, derive the fundamental frequencies of the beam and thus obtain explicit analytical solutions [1–4]. Although this approach is highly efficient when applicable, the analysis becomes significantly more complex when discontinuous beam parameters and general dynamic loads are required. An alternative is to utilize numerical methods. In [5] the spatial component of the solution is discretized with compact finite differences and used to numerically derive the natural frequencies of nanobeams. However, this approach assumes that the spatial and temporal parts of the solution function can be separated. In this paper we solve the DBE numerically in the time domain using the *method of lines*, i.e. we discretize the partial differential equation (PDE) in space and then solve the resulting system of ordinary differential equations (ODE). The spatial discretization is done using high-order explicit finite difference methods. This approach is not limited by any specific choice of boundary condi-

* Corresponding author.
E-mail address: gustav.eriksson@it.uu.se (G. Eriksson).

https://doi.org/10.1016/j.jcp.2023.111907

tion or external loads and does not assume that the solution takes any particular form (e.g. separate temporal and spatial components).

It has for a long time been known that non-trivial boundary procedures are required to obtain stable high-order finite difference discretizations of initial-boundary value problems (IBVP) [6–10]. One way to manage this is to combine *summation by parts* (SBP) finite difference operators with either the *simultaneous approximation term* (SAT) method or the *projection* (P) method to impose boundary conditions. With both SBP-SAT and SBP-P semi-discrete energy estimates that mimic the continuous estimates can be derived, proving that the ODE systems are stable. The SBP-SAT and SBP-P methods have been applied to various PDE:s in the past, see for example [11–15]. See also [16–18] for examples of the SBP-SAT method applied to IBVP:s involving third and fourth derivatives. In [16] the SBP-SAT method was used to solve the DBE with constant coefficients.

In this paper, we begin by deriving stable SBP-P discretizations of the DBE with clamped and free boundary conditions and compare them to previously presented SBP-SAT discretizations [16]. We then consider the DBE with piecewise constant coefficients, requiring additional interface conditions to couple the solution across the discontinuities. We present novel SBP-SAT, SBP-P, and hybrid SBP-SAT-P discretizations for this problem and compare them numerically in terms of accuracy and computational efficiency. Previously SBP-SAT and SBP-P have been used to impose interface conditions for PDE:s with second derivatives in space, see for example [12,14,19]. Here we propose a novel third alternative utilizing SAT and projection simultaneously, SBP-SAT-P, where some interface conditions are imposed using SAT and others using projection. The focus of the current work is twofold: a): to develop a stable method for solving the DBE with general parameters, boundary conditions, and external loads and b): to compare SBP-SAT, SBP-P, and SBP-SAT-P for a problem involving high spatial derivatives (for which it is traditionally difficult to derive energy stable schemes). The methods developed in this paper can almost directly be applied to two-dimensional problems. To show this, we also present an SBP-SAT-P discretization of the dynamic Kirchoff-Love plate equation, which is an extension of the beam equation to two-dimensional plates.

This paper is organized as follows: In Section 2 the DBE is introduced. In Section 3 necessary definitions are presented. In Sections 4 and 5 the DBE with constant and piecewise constant coefficients respectively is analyzed. In Section 6 the time stepping scheme is presented. In Section 7 the methods for the DBE are compared and the analysis is verified numerically. In Section 8 the Kirchoff-Love plate equation is considered. Conclusions are drawn in Section 9.

2. The dynamic beam equation

Denote by $w(x,t)$ the beam's deflection from the x-axis, the DBE is then given by

$$\begin{aligned}
&\mu(x)\frac{\partial^2 w(x,t)}{\partial t^2} = -\frac{\partial^2}{\partial x^2}\left(E(x)I(x)\frac{\partial^2 w(x,t)}{\partial x^2}\right) + q(x,t), && x_l \le x \le x_r, \quad t > 0,\\
&w(x,t) = f_1(x), \quad \frac{\partial w(x,t)}{\partial t} = f_2(x), && x_l \le x \le x_r, \quad t = 0,\\
&B_L(w) = \mathbf{G}_L(t), && x = x_l, \qquad t > 0,\\
&B_R(w) = \mathbf{G}_R(t), && x = x_r, \qquad t > 0,
\end{aligned} \tag{1}$$

where $E(x)$ is the elastic modulus of the beam, $I(x)$ is the second moment of area of the beam's cross-section, $\mu(x)$ is the mass per unit length and $q(x,t)$ is the external load. The initial data is $f_{1,2}(x)$. The boundary operators $B_{L,R}$ and boundary data $\mathbf{G}_{L,R}(t)$ determine the boundary conditions. For notational clarity, we rewrite the PDE as

$$b(x)u_{tt} = -(a(x)u_{xx})_{xx} + F(x,t), \tag{2}$$

where subscripts denote partial differentiation. Note that the functions $a(x) = E(x)I(x)$ and $b(x) = \mu(x)$ are positive. Throughout this paper, we will assume that the boundary data $\mathbf{G}_{L,R}(t)$ and forcing function $F(x,t)$ are zero (all methods considered are equally applicable with general non-homogeneous data).

3. Definitions

Let the inner product of two real-valued functions $u, v \in L^2[x_l, x_r]$ be defined by $(u,v) = \int_{x_l}^{x_r} uv\,dx$ and the corresponding norm by $\|u\|^2 = (u,u)$.

The domain is discretized into m equidistant grid points given by

$$x_i = x_l + (i-1)h, \quad i = 1,2,...,m, \quad h = \frac{x_r - x_l}{m-1}. \tag{3}$$

A semi-discrete solution vector is given by $v = [v_1, v_2, ..., v_m]^\top$, where v_i is the approximate solution at grid point x_i. Let $(u,v)_H = u^\top Hv$, where $H = H^\top > 0$, define a discrete inner product for discrete real-valued vectors $u, v \in \mathbb{R}^m$, and $\|v\|_H^2 = v^\top Hv$ the corresponding norm. We also define

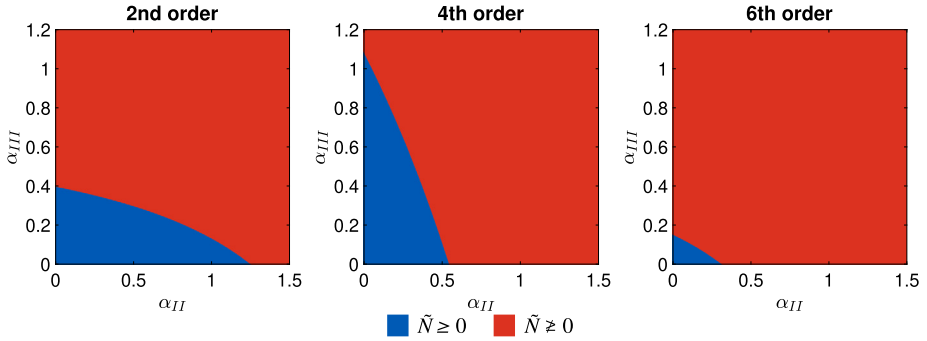

Fig. 1. Influence of parameters α_{II} and α_{III} on definiteness of $\tilde{N}$.

$$\bar{H} = \begin{bmatrix} H & 0 \\ 0 & H \end{bmatrix}. \tag{4}$$

The SBP operators used here are central finite difference operators with boundary closures carefully designed to mimic integration-by-parts in the semi-discrete setting. In this paper we present results for the 2nd, 4th and 6th order accurate fourth-derivative SBP operators presented in [18], the following definition is central:

Definition 1. A difference operator $D_4 = H^{-1}\left(N + e_l d_{3;l}^\top + d_{1;l} d_{2;l}^\top + e_r d_{3;r}^\top - d_{1;r} d_{2;r}^\top\right)$ approximating $\partial^4/\partial x^4$ using a pth-order accurate narrow-stencil in the interior is said to be a pth-order diagonal-norm fourth-derivative SBP operator if $H = H^\top > 0$ is diagonal, $N = N^T \geq 0$, $d_{1;l}^\top v \approx -u_x|^l$, $d_{1;r}^\top v \approx u_x|^r$, $d_{2;l}^\top v \approx -u_{xx}|^l$, $d_{2;r}^\top v \approx u_{xx}|^r$, $d_{3;l}^\top v \approx -u_{xxx}|^l$ and $d_{3;r}^\top v \approx u_{xxx}|^r$ are finite difference approximations of the first, second and third normal derivatives at the left and right boundary points and e_l and e_r are the first and last columns of the identity matrix, respectively.

For the Kirchoff-Love plate problem in Section 8, both second- and fourth-derivative SBP operators constructed from the same norm (H) are needed, in order to discretize the cross-derivative terms. Second derivative SBP operators were also presented in [18], with the following definition:

Definition 2. A difference operator $D_2 = H^{-1}(-M + e_l d_{1;l}^\top + e_r d_{1;r}^\top)$ approximating $\partial^2/\partial x^2$ using a pth-order accurate narrow-stencil is said to be a pth-order accurate narrow-stencil diagonal-norm second derivative SBP operator if H is diagonal and positive definite, M is symmetric and positive semi-definite, $d_{1;l}^\top v \approx -u_x|^l$, $d_{1;r}^\top v \approx u_x|^r$ are finite difference approximations of the first normal derivative at the left and right boundary points and e_l and e_r are the first and last columns of the identity matrix, respectively.

The matrix N can be decomposed in the following way:

$$N = \tilde{N} + h\alpha_{II}\left(d_{2;l} d_{2;l}^\top + d_{2;r} d_{2;r}^\top\right) + h^3 \alpha_{III}\left(d_{3;l} d_{3;l}^\top + d_{3;r} d_{3;r}^\top\right), \tag{5}$$

where $\tilde{N} = \tilde{N}^\top \geq 0$ and α_{II} and α_{III} are positive constants not dependent on h. In Fig. 1 the values ensuring positive semi-definiteness of $\tilde{N}$ are presented for the 2nd, 4th and 6th order accurate SBP operators used here.

4. Homogeneous beam

4.1. Well-posedness

We begin by considering a homogeneous beam, i.e. $a(x)$ and $b(x)$ are constant functions. Multiplying (2) by u_t, integrating over the domain, and using integration by parts (the energy method) leads to

$$\frac{d}{dt} E = 2a[-u_t u_{xxx} + u_{tx} u_{xx}]_{x_l}^{x_r}, \tag{6}$$

where E is an energy defined as

$$E = b\|u_t\|^2 + a\|u_{xx}\|^2. \tag{7}$$

Assuming existence, well-posedness of (2) is achieved by imposing the minimum number of boundary conditions such that the right-hand side in (6) is non-positive with zero boundary data, i.e. the energy for the homogeneous problem is non-increasing. For this problem, the minimum number of boundary conditions is two on each boundary [16]. In this paper we consider the following homogeneous boundary conditions:

$$\begin{aligned} &\textit{clamped:} && u = 0, && u_x = 0, && x = x_{l,r}, \\ &\textit{free:} && u_{xx} = 0, && u_{xxx} = 0, && x = x_{l,r}. \end{aligned} \tag{8}$$

Either combination of these lead to energy conservation,

$$\frac{d}{dt} E = 0. \tag{9}$$

4.2. Spatial discretization

A semi-discrete SBP discretization of (2) with constant a and b is

$$b v_{tt} = -a D_4 v. \tag{10}$$

The semi-discrete formulations of the boundary conditions (8) are

$$\begin{aligned} &\textit{clamped:} && e_l^\top v = 0, && d_{1;l}^\top v = 0, && e_r^\top v = 0, && d_{1;r}^\top v = 0, \\ &\textit{free:} && d_{2;l}^\top v = 0, && d_{3;l}^\top v = 0, && d_{2;r}^\top v = 0, && d_{3;r}^\top v = 0. \end{aligned} \tag{11}$$

To impose the boundary conditions while simultaneously obtaining a stable ODE, we consider two methods: SAT and projection. With SAT the ODE system takes the form

$$b v_{tt} = -a D_4 v + SAT, \tag{12}$$

where $SAT = aH^{-1} B v$ and B is a carefully chosen term so that the boundary conditions are imposed and an energy estimate is obtained, i.e. the eigenvalues of the matrix $-aD_4 + aH^{-1}B$ are real and non-positive. Stable SBP-SAT discretizations of the DBE with clamped and free boundary conditions are derived in [16]. To make the paper self-contained, we also present them here.

The projection method augments the system (10) as

$$b v_{tt} = -a P D_4 P v, \tag{13}$$

where P is a projection from $\mathbb{R}^m$ onto a subspace where the boundary conditions are satisfied. If P is an orthogonal projection with respect to the inner product $(\cdot, \cdot)_H$, i.e.

$$(Pu, v)_H = (u, Pv)_H, \quad u, v \in \mathbb{R}^m, \tag{14}$$

the energy method can be used to show that the eigenvalues of the matrix $-aPD_4P$ are real and non-positive. For the derivation of P and examples of using the projection method for imposing boundary conditions, see [12,13,20,21].

In Sections 4.3-4.6 we derive semi-discrete energy estimates for (10) with boundary conditions (11) imposed using SAT and projection. To make the analysis more readable, we only present boundary terms corresponding to the left boundary. The right boundary terms are done analogously.

Remark 1. In this work, we only consider homogeneous boundary conditions. For inhomogeneous boundary conditions additional time-dependent data terms are included in (12) and (13). Boundary and forcing data do not affect stability.

4.3. Clamped boundary conditions with SAT

SAT for clamped boundary conditions, first presented in Lemma 4.3 in [16], is given by

$$SAT_c = -aH^{-1}(d_{3;l} + h^{-3}\tau_l e_l) e_l^\top v - aH^{-1}(d_{2;l} + h^{-1}\sigma_l d_{1;l}) d_{1;l}^\top v, \tag{15}$$

where τ_l and σ_l are constants chosen for stability. For completeness, we restate the Lemma and stability proof here.

Lemma 1. *The system* (12) *is a stable approximation of the DBE with clamped boundary conditions if SAT is given by* (15) *and*

$$\tau_l = \frac{1}{\alpha_{III}} \quad \textit{and} \quad \sigma_l = \frac{1}{\alpha_{II}}. \tag{16}$$

Proof. The energy method applied to (12) with SAT given by (15) together with (5) leads to

$$\frac{d}{dt} E = 0, \tag{17}$$

where

$$E = b\|v_t\|_H^2 + a(v^\top \tilde{N} v + w^\top A w), \tag{18}$$

$$w = \begin{bmatrix} e_l^\top v \\ d_{3;l}^\top v \\ d_{1;l}^\top v \\ d_{2;l}^\top v \end{bmatrix} \quad \text{and} \quad A = \begin{bmatrix} h^{-3}\tau_l & 1 & 0 & 0 \\ 1 & h^3\alpha_{III} & 0 & 0 \\ 0 & 0 & h^{-1}\sigma_l & 1 \\ 0 & 0 & 1 & h\alpha_{II} \end{bmatrix}. \tag{19}$$

For E to be a valid energy it must be positive semi-definite. The matrix $\tilde{N}$ is positive semi-definite for specific choices of α_{II} and α_{III}, see Fig. 1. It remains to show which τ_l and σ_l lead to positive semi-definite A. By applying Sylvester's criterion we get the conditions

$$\tau_l = \frac{1}{\alpha_{III}} \quad \text{and} \quad \sigma_l = \frac{1}{\alpha_{II}}. \quad \square \tag{20}$$

Note that multiple choices of α_{II} and α_{III} lead to stability.

4.4. Clamped boundary conditions with projection

The semi-discrete clamped boundary conditions can be written as $L_c v = 0$ where

$$L_c = \begin{bmatrix} e_l^\top \\ d_{1;l}^\top \end{bmatrix}. \tag{21}$$

The projection operator is given by

$$P = I_m - H^{-1} L_c^\top (L_c H^{-1} L_c^\top)^{-1} L_c, \tag{22}$$

where I is the $m \times m$ identity matrix. The following Lemma is one of the main results of this work:

Lemma 2. *The system (13) is a stable approximation of the DBE with clamped boundary conditions if the projection operator P is given by (22).*

Proof. The energy method applied to (13) leads to

$$b(v_t, v_{tt})_H = -a(Pv_t, D_4 Pv)_H, \tag{23}$$

where the self-adjoint property (14) is used. Let $\tilde{v} = Pv$ denote the projected solution vector and use Definition 1, we get

$$\frac{d}{dt}E = -2a(e_l^\top \tilde{v}_t d_{3;l}^\top \tilde{v} + d_{1;l}^\top \tilde{v}_t d_{2;l}^\top \tilde{v}), \tag{24}$$

where

$$E = b\|v_t\|_H^2 + a\tilde{v}^\top N \tilde{v} \tag{25}$$

defines an energy. Since $L_c \tilde{v} = L_c P v = 0$ we have $e_l^\top \tilde{v} = d_{1;l}^\top \tilde{v} = 0$ and thus

$$\frac{d}{dt}E = 0. \quad \square \tag{26}$$

4.5. Free boundary conditions with SAT

SAT for free boundary conditions, first presented in Lemma 4.2 in [16], are given by

$$SAT_f = a\tau_l H^{-1} d_{1;l} d_{2;l}^\top v + a\sigma_l H^{-1} e_l d_{3;l}^\top v, \tag{27}$$

where τ_l and σ_l are constants chosen for stability. For completeness, we restate the Lemma and stability proof here.

Lemma 3. *The system (12) is a stable approximation of the DBE with free boundary conditions if SAT is given by (27) and*

$$\tau_l = \sigma_l = 1. \tag{28}$$

Proof. The energy method applied to (12) with SAT given by (27) leads to

$$\frac{d}{dt}E = 2a(\tau_l - 1)d_{1;l}^\top v_t d_{2;l}^\top v + 2a(\sigma_l - 1)e_l^\top v_t d_{3;l}^\top v, \tag{29}$$

where

$$E = b\|v_t\|_H^2 + av^\top Nv \tag{30}$$

defines an energy. The choice $\tau_l = \sigma_l = 1$ results in

$$\frac{d}{dt}E = 0. \quad \square \tag{31}$$

4.6. Free boundary conditions with projection

The semi-discrete free boundary conditions can be written as $L_f v = 0$ where

$$L_f = \begin{bmatrix} d_{2;l}^\top \\ d_{3;l}^\top \end{bmatrix}. \tag{32}$$

The projection operator is given by

$$P = I_m - H^{-1}L_f^\top (L_f H^{-1} L_f^\top)^{-1} L_f, \tag{33}$$

where I is the $m \times m$ identity matrix. The following Lemma is one of the main results in this work:

Lemma 4. *The system* (13) *is a stable approximation of the DBE with free boundary conditions if the projection operator P is given by* (33).

Proof. The energy method applied to (13) leads to

$$b(v_t, v_{tt})_H = -a(Pv_t, D_4 Pv)_H, \tag{34}$$

where the self-adjoint property (14) is used. Let $\tilde{v} = Pv$ denote the projected solution vector and use Definition 1, we get

$$\frac{d}{dt}E = -2a(e_l^\top \tilde{v}_t d_{3;l}^\top \tilde{v} + d_{1;l}^\top \tilde{v}_t d_{2;l}^\top \tilde{v}), \tag{35}$$

where

$$E = b\|v_t\|_H^2 + a\tilde{v}^\top N\tilde{v}, \tag{36}$$

defines an energy. Since $L_f \tilde{v} = L_f Pv = 0$ we have $d_{2;l}^\top \tilde{v} = d_{3;l}^\top \tilde{v} = 0$ and thus

$$\frac{d}{dt}E = 0. \quad \square \tag{37}$$

5. Piecewise homogeneous beam

In this section, we turn to the DBE with piecewise constant coefficients. In the analysis, we assume that $x_l < 0$ and $x_r > 0$ and consider (2) with $a(x)$ and $b(x)$ piecewise constant with a discontinuity at $x = 0$, i.e.

$$a(x) = \begin{cases} a^{(1)}, & \text{if } x < 0 \\ a^{(2)}, & \text{if } x > 0 \end{cases}, \quad b(x) = \begin{cases} b^{(1)}, & \text{if } x < 0 \\ b^{(2)}, & \text{if } x > 0 \end{cases}, \tag{38}$$

where $a^{(1,2)}$ and $b^{(1,2)}$ are positive constants. We begin by deriving well-posed interface conditions in the continuous setting, we then discretize the equations in space and derive stable semi-discrete formulations with the interface conditions imposed using SAT, projection, and hybrid SAT and projection.

5.1. Well-posedness

The energy method applied to (2) with $a(x)$ and $b(x)$ given by (38) leads to

$$\frac{d}{dt}E^{(a,b)} = a^{(1)}[u_{tx}u_{xx} - u_t u_{xxx}]_{x_l}^{0^-} + a^{(2)}[u_{tx}u_{xx} - u_t u_{xxx}]_{0^+}^{x_r}, \tag{39}$$

where

$$E^{(a,b)} = \int_{x_l}^{0^-} b^{(1)}u_t^2 + a^{(1)}u_{xx}^2\,dx + \int_{0^+}^{x_r} b^{(2)}u_t^2 + a^{(2)}u_{xx}^2\,dx, \tag{40}$$

defines an energy. To obtain an energy estimate we split $u(x,t)$ at the interface such that

$$u(x,t) = \begin{cases} u^{(1)}(x,t), & \text{if } x < 0 \\ u^{(2)}(x,t), & \text{if } x > 0 \end{cases}, \tag{41}$$

and rewrite (2) as a system of PDEs:

$$\begin{aligned} b^{(1)}u_{tt}^{(1)} &= -a^{(1)}u_{xxxx}^{(1)}, \qquad x_l \le x \le 0, \quad t > 0, \\ b^{(2)}u_{tt}^{(2)} &= -a^{(2)}u_{xxxx}^{(2)}, \qquad 0 \le x \le x_r, \quad t > 0. \end{aligned} \tag{42}$$

The energy estimate becomes

$$\frac{d}{dt}E^{(a,b)} = a^{(1)}[u_{tx}^{(1)}u_{xx}^{(1)} - u_t^{(1)}u_{xxx}^{(1)}]_{x_l}^{0} + a^{(2)}[u_{tx}^{(2)}u_{xx}^{(2)} - u_t^{(2)}u_{xxx}^{(2)}]_{0}^{x_r}, \tag{43}$$

where

$$E^{(a,b)} = b^{(1)}\|u_t^{(1)}\|^2 + b^{(2)}\|u_t^{(2)}\|^2 + a^{(1)}\|u_{xx}^{(1)}\|^2 + a^{(2)}\|u_{xx}^{(2)}\|^2. \tag{44}$$

In addition to outer boundary conditions, the following *interface conditions* will bound the energy:

$$\begin{aligned} u^{(1)} &= u^{(2)}, & x = 0, \\ u_x^{(1)} &= u_x^{(2)}, & x = 0, \\ a^{(1)}u_{xx}^{(1)} &= a^{(2)}u_{xx}^{(2)}, & x = 0, \\ a^{(1)}u_{xxx}^{(1)} &= a^{(2)}u_{xxx}^{(2)}, & x = 0. \end{aligned} \tag{45}$$

With either boundary conditions in (8) and the interface conditions (45) the energy given by (44) is conserved.

5.2. Spatial discretization

Let $v^{(1)}$ and $v^{(2)}$ denote solution vectors on the left and right sides of the discontinuity respectively. For notational clarity, we assume that the same SBP operators are used in both blocks. A consistent semi-discrete formulation of (42) is given by

$$(B \otimes I_m)w_{tt} = -(A \otimes D_4)w, \tag{46}$$

where

$$w = \begin{bmatrix} v^{(1)} \\ v^{(2)} \end{bmatrix}, \quad B = \begin{bmatrix} b^{(1)} & 0 \\ 0 & b^{(2)} \end{bmatrix}, \quad A = \begin{bmatrix} a^{(1)} & 0 \\ 0 & a^{(2)} \end{bmatrix},$$

and $\otimes$ denotes the Kronecker product. The semi-discrete formulation of the interface conditions (45) is

$$\begin{aligned} e_r^\top v^{(1)} - e_l^\top v^{(2)} &= 0, \\ d_{1;r}^\top v^{(1)} + d_{1;l}^\top v^{(2)} &= 0, \\ a^{(1)}d_{2;r}^\top v^{(1)} + a^{(2)}d_{2;l}^\top v^{(2)} &= 0, \\ a^{(1)}d_{3;r}^\top v^{(1)} + a^{(2)}d_{3;l}^\top v^{(2)} &= 0. \end{aligned} \tag{47}$$

In the analysis of the semi-discrete multiblock problem, we assume that outer boundary conditions are imposed correctly (for example by using any of the methods discussed in Sections 4.3-4.6). Therefore, the terms corresponding to outer boundaries are not included in the equations presented.

As for the single-block problem, the semi-discrete interface conditions (47) should be imposed such that an energy estimate is obtained. With SBP-SAT additional terms are added to (46). With SBP-P the system (46) is augmented similarly as (13), using a projection onto the subspace of $\mathbb{R}^{2m}$ where the interface conditions (47) are fulfilled. Since the dual-block projection operator acts on the full solution vector w, the self-adjoint property becomes

$$(Pu, v)_{\tilde{H}} = (u, Pv)_{\tilde{H}}, \quad u, v \in \mathbb{R}^{2m}. \tag{48}$$

With SBP-SAT-P both SAT and projection are used to modify the system simultaneously. In Sections 5.3-5.5 semi-discrete formulations and stability proofs of each of the three methods are presented.

5.3. Interface conditions with SAT

A consistent semi-discrete approximation of (42) with the interface conditions (45) imposed using the SAT method is given by

$$(B \otimes I_m) w_{tt} = -(A \otimes D_4) w + SAT, \tag{49}$$

where $SAT = SAT_1 + SAT_2 + SAT_3 + SAT_4$,

$$\begin{aligned}
SAT_1 &= \begin{bmatrix} -H^{-1}(\frac{\tau}{h^3}e_r + \frac{a^{(1)}}{2}d_{3;r})e_r^\top & H^{-1}(\frac{\tau}{h^3}e_r + \frac{a^{(1)}}{2}d_{3;r})e_l^\top \\ H^{-1}(\frac{\tau}{h^3}e_l + \frac{a^{(2)}}{2}d_{3;l})e_r^\top & -H^{-1}(\frac{\tau}{h^3}e_l + \frac{a^{(2)}}{2}d_{3;l})e_l^\top \end{bmatrix} w, \\
SAT_2 &= \begin{bmatrix} -H^{-1}(\frac{\sigma}{h}d_{1;r} - \frac{a^{(1)}}{2}d_{2;r})d_{1;r}^\top & -H^{-1}(\frac{\sigma}{h}d_{1;r} - \frac{a^{(1)}}{2}d_{2;r})d_{1;l}^\top \\ -H^{-1}(\frac{\sigma}{h}d_{1;l} + \frac{a^{(2)}}{2}d_{2;l})d_{1;r}^\top & -H^{-1}(\frac{\sigma}{h}d_{1;l} + \frac{a^{(2)}}{2}d_{2;l})d_{1;l}^\top \end{bmatrix} w, \\
SAT_3 &= \begin{bmatrix} -\frac{a^{(1)}}{2}H^{-1}d_{1;r}d_{2;r}^\top & -\frac{a^{(2)}}{2}H^{-1}d_{1;r}d_{2;l}^\top \\ \frac{a^{(1)}}{2}H^{-1}d_{1;l}d_{2;r}^\top & \frac{a^{(2)}}{2}H^{-1}d_{1;l}d_{2;l}^\top \end{bmatrix} w, \\
SAT_4 &= \begin{bmatrix} \frac{a^{(1)}}{2}H^{-1}e_r d_{3;r}^\top & \frac{a^{(2)}}{2}H^{-1}e_r d_{3;l}^\top \\ \frac{a^{(1)}}{2}H^{-1}e_l d_{3;r}^\top & \frac{a^{(2)}}{2}H^{-1}e_l d_{3;l}^\top \end{bmatrix} w,
\end{aligned} \tag{50}$$

and τ and σ are parameters tuned for stability. The ansatz for the SAT in (49) is similar in structure to the SAT presented in [19] for imposing interface conditions for the second-order wave equation. The following Lemma is one of the main results of this paper:

Lemma 5. *The system (49) is a stable approximation of the DBE with piecewise constant parameters if*

$$\tau = \frac{1}{4\alpha_{III}}(a^{(1)} + a^{(2)}), \quad \sigma = \frac{1}{4\alpha_{II}}(a^{(1)} + a^{(2)}), \tag{51}$$

and α_{II} and α_{III} are chosen so that $\tilde{N}$ is positive semi-definite.

Proof. The energy method applied to (49) together with (5) and Definition 1 leads to

$$\frac{d}{dt}E = 0, \tag{52}$$

where

$$\begin{aligned}
E = {} & b^{(1)}\|v_t^{(1)}\|_H^2 + b^{(2)}\|v_t^{(2)}\|_H^2 + a^{(1)}(v^{(1)})^\top \tilde{N} v^{(1)} + a^{(2)}(v^{(2)})^\top \tilde{N} v^{(2)} \\
& + (w^{(1)})^\top A_1 w^{(1)} + (w^{(2)})^\top A_2 w^{(2)},
\end{aligned} \tag{53}$$

and

$$\begin{aligned}
w_1 &= \begin{bmatrix} e_r^\top v^{(1)} \\ d_{3;r}^\top v^{(1)} \\ e_l^\top v^{(2)} \\ d_{3;l}^\top v^{(2)} \end{bmatrix}, \quad A_1 = \begin{bmatrix} \frac{\tau}{h^3} & \frac{a^{(1)}}{2} & \frac{-\tau}{h^3} & \frac{-a^{(2)}}{2} \\ \frac{a^{(1)}}{2} & a^{(1)}h^3\alpha_{III} & \frac{-a^{(1)}}{2} & 0 \\ \frac{-\tau}{h^3} & \frac{-a^{(1)}}{2} & \frac{\tau}{h^3} & \frac{a^{(2)}}{2} \\ \frac{-a^{(2)}}{2} & 0 & \frac{a^{(2)}}{2} & a^{(2)}h^3\alpha_{III} \end{bmatrix}, \\
w_2 &= \begin{bmatrix} d_{1;r}^\top v^{(1)} \\ d_{2;r}^\top v^{(1)} \\ d_{1;l}^\top v^{(2)} \\ d_{2;l}^\top v^{(2)} \end{bmatrix}, \quad A_2 = \begin{bmatrix} \frac{\sigma}{h} & \frac{-a^{(1)}}{2} & \frac{\sigma}{h} & \frac{a^{(2)}}{2} \\ \frac{-a^{(1)}}{2} & a^{(1)}h\alpha_{II} & \frac{-a^{(1)}}{2} & 0 \\ \frac{\sigma}{h} & \frac{-a^{(1)}}{2} & \frac{\sigma}{h} & \frac{a^{(2)}}{2} \\ \frac{a^{(2)}}{2} & 0 & \frac{a^{(2)}}{2} & a^{(2)}h\alpha_{II} \end{bmatrix}.
\end{aligned} \tag{54}$$

For E to be a valid energy it must be positive semi-definite. The matrix $\tilde{N}$ is positive semi-definite for specific choices of α_{II} and α_{III}, see Fig. 1. It remains to show which τ and σ lead to positive semi-definite A_1 and A_2. By Sylvester's criterion we get the conditions

$$\tau = \frac{1}{4\alpha_{III}}(a^{(1)} + a^{(2)}) \quad \text{and} \quad \sigma = \frac{1}{4\alpha_{II}}(a^{(1)} + a^{(2)}). \quad \square \tag{55}$$

Note that multiple choices of α_{II} and α_{III} lead to stability.

5.4. Interface conditions with projection

A consistent semi-discrete approximation of (42) with the interface conditions (45) imposed using the projection method is given by

$$(B \otimes I_m) w_{tt} = -P(A \otimes D_4) P w, \tag{56}$$

where

$$P = I_{2m} - \bar{H}^{-1} L^\top (L \bar{H}^{-1} L^\top)^{-1} L, \tag{57}$$

I_{2m} is the $2m \times 2m$ identity matrix and L is given by

$$L = \begin{bmatrix} e_r^\top & -e_l^\top \\ d_{1;r}^\top & d_{1;l}^\top \\ a^{(1)} d_{2;r}^\top & a^{(2)} d_{2;l}^\top \\ a^{(1)} d_{3;r}^\top & a^{(2)} d_{3;l}^\top \end{bmatrix}. \tag{58}$$

Note that $Lw = 0$ defines the interface conditions (47). The following Lemma is one of the main results of this paper:

Lemma 6. *The system (56) is a stable approximation of the DBE with piecewise constant parameters.*

Proof. The energy method applied to (56) leads to

$$(w_t, (B \otimes I_m) w_{tt})_{\bar{H}} = -(P w_t, (A \otimes D_4) P w)_{\bar{H}}, \tag{59}$$

where the self-adjoint property (48) is used. Let $\tilde{w} = \begin{bmatrix} \tilde{v}^{(1)} \\ \tilde{v}^{(2)} \end{bmatrix} = Pw$ denote the projected solution and use Definition 1, we get

$$\begin{aligned} \frac{d}{dt} E = &-2a^{(1)} (e_r^\top \tilde{v}_t^{(1)} d_{3;r}^\top \tilde{v}^{(1)} - d_{1;r}^\top \tilde{v}_t^{(1)} d_{2;r}^\top \tilde{v}^{(1)}) \\ &- 2a^{(2)} (e_l^\top \tilde{v}_t^{(2)} d_{3;l}^\top \tilde{v}^{(2)} + d_{1;l}^\top \tilde{v}_t^{(2)} d_{2;l}^\top \tilde{v}^{(2)}), \end{aligned} \tag{60}$$

where

$$E = b^{(1)} \| v_t^{(1)} \|_H^2 + b^{(2)} \| v_t^{(2)} \|_H^2 + a^{(1)} (\tilde{v}^{(1)})^\top N \tilde{v}^{(1)} + a^{(2)} (\tilde{v}^{(2)})^\top N \tilde{v}^{(2)}, \tag{61}$$

defines an energy. Since $L\tilde{w} = LPw = 0$, i.e. the interface conditions (47) are fulfilled for $\tilde{v}^{(1)}$ and $\tilde{v}^{(2)}$, the terms in the right-hand side of (60) cancel and we get

$$\frac{d}{dt} E = 0. \quad \square \tag{62}$$

5.5. Interface conditions with hybrid SAT and projection

A consistent semi-discrete approximation of (42) with the first two interface conditions in (45) imposed using the projection method and the last two using the SAT method is given by

$$(B \otimes I_m) w_{tt} = -P(A \otimes D_4) P w + SAT, \tag{63}$$

where $SAT = SAT_1 + SAT_2$,

$$
\begin{aligned}
SAT_1 &= P \begin{bmatrix} -\frac{a^{(1)}}{2} H^{-1} d_{1;r} d_{2;r}^\top & -\frac{a^{(2)}}{2} H^{-1} d_{1;r} d_{2;l}^\top \\ \frac{a^{(1)}}{2} H^{-1} d_{1;l} d_{2;r}^\top & \frac{a^{(2)}}{2} H^{-1} d_{1;l} d_{2;l}^\top \end{bmatrix} Pw, \\
SAT_2 &= P \begin{bmatrix} \frac{a^{(1)}}{2} H^{-1} e_r d_{3;r}^\top & \frac{a^{(2)}}{2} H^{-1} e_r d_{3;l}^\top \\ \frac{a^{(1)}}{2} H^{-1} e_l d_{3;r}^\top & \frac{a^{(2)}}{2} H^{-1} e_l d_{3;l}^\top \end{bmatrix} Pw.
\end{aligned} \tag{64}
$$

The projection operator is given by

$$
P = I_{2m} - \bar{H}^{-1} L^\top (L \bar{H}^{-1} L^\top)^{-1} L, \tag{65}
$$

where

$$
L = \begin{bmatrix} e_r^\top & -e_l^\top \\ d_{1;r}^\top & d_{1;l}^\top \end{bmatrix}. \tag{66}
$$

Note that since P appears in (64) the SAT is weakly imposing the interface conditions in the subspace of projected solutions. The following Lemma is one of the main results of this paper:

Lemma 7. *The system* (63) *is a stable approximation of the DBE with piecewise constant parameters.*

Proof. The energy method applied to (63) leads to

$$
(w_t, (B \otimes I_m) w_{tt})_{\bar{H}} = -(w_t, P(A \otimes D_4) Pw + SAT)_{\bar{H}}. \tag{67}
$$

Let $\tilde{w} = \begin{bmatrix} \tilde{v}^{(1)} \\ \tilde{v}^{(2)} \end{bmatrix} = Pw$ denote the projected solution. Using the self-adjoint property (48) and Definition 1 results in

$$
\begin{aligned}
\frac{d}{dt} E = {} & a^{(1)} (e_l^\top \tilde{v}_t^{(2)} - e_r^\top \tilde{v}_t^{(1)}) d_{3;r}^\top \tilde{v}^{(1)} + a^{(1)} (d_{1;l}^\top \tilde{v}_t^{(2)} + d_{1;r}^\top \tilde{v}_t^{(1)}) d_{2;r}^\top \tilde{v}^{(1)} \\
& - a^{(2)} (e_l^\top \tilde{v}_t^{(2)} - e_r^\top \tilde{v}_t^{(1)}) d_{3;l}^\top \tilde{v}^{(2)} - a^{(2)} (d_{1;l}^\top \tilde{v}_t^{(2)} + d_{1;r}^\top \tilde{v}_t^{(1)}) d_{2;l}^\top \tilde{v}^{(2)}
\end{aligned} \tag{68}
$$

where

$$
E = b^{(1)} \| v_t^{(1)} \|_H^2 + b^{(2)} \| v_t^{(2)} \|_H^2 + a^{(1)} (\tilde{v}^{(1)})^\top N \tilde{v}^{(1)} + a^{(2)} (\tilde{v}^{(2)})^\top N \tilde{v}^{(2)}, \tag{69}
$$

defines an energy. Since $L\tilde{w} = LPv = 0$ we have $e_r^\top \tilde{v}^{(1)} = e_l^\top \tilde{v}^{(2)}$ and $d_{1;r}^\top \tilde{v}^{(1)} = -d_{1;l}^\top \tilde{v}^{(2)}$. Substituted into (68) gives

$$
\frac{d}{dt} E = 0. \quad \square \tag{70}
$$

6. Time integration

All methods considered in this paper lead to a system of ODE:s (with m and $2m$ unknowns for the single- and dual-block problems respectively) on the form

$$
\begin{aligned}
v_{tt} &= Dv, \qquad t \geq 0 \\
v(t) &= f_1, \qquad t = 0, \\
v_t(t) &= f_2, \qquad t = 0,
\end{aligned} \tag{71}
$$

where D is a matrix with real non-positive eigenvalues. To integrate the system in time we use a 4th order accurate method given by

$$
\begin{aligned}
v^{(0)} &= f_1, \\
v^{(1)} &= (I + \frac{k^2}{2} D) f_1 + k (I + \frac{k^2}{6} D) f_2, \\
v^{(n+1)} &= (2I + k^2 D + \frac{k^4}{12} DD) v^{(n)} - v^{(n-1)},
\end{aligned} \tag{72}
$$

where k is the temporal step size. See [12,16] for more details on these types of time-stepping methods. It is easily shown that stability is obtained if k satisfies

$$
k^2 \rho(D) < 12, \tag{73}
$$

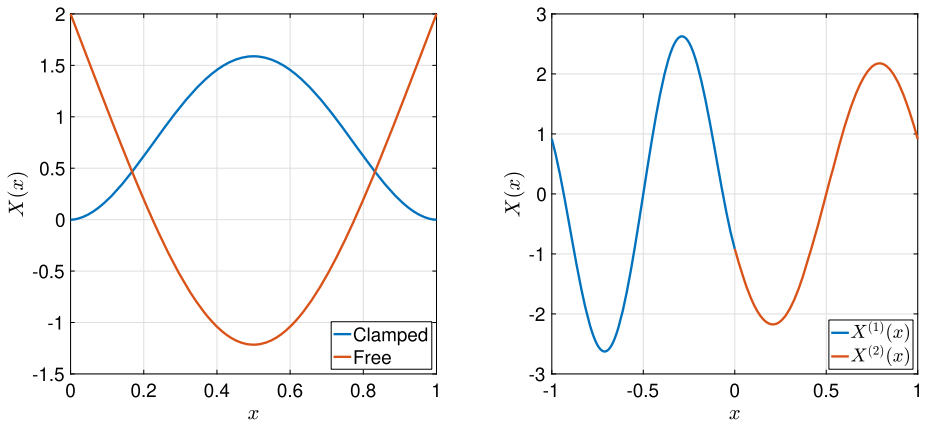

Fig. 2. Left: Initial functions $X(x)$ for the homogeneous beam problem with clamped and free boundary conditions. Right: Initial functions $X^{(1,2)}(x)$ for the piecewise homogeneous beam problem with interface conditions at $x = 0$ and $x = \pm 1$.

where $\rho(D)$ is the spectral radius of D. Introducing the undivided matrix $\tilde{D} = h^4 D$ we get the CFL condition

$$k < \sqrt{\frac{12}{\rho(\tilde{D})}} h^2. \tag{74}$$

The spectral radius of the undivided operator $\tilde{D}$ is dependent on the spatial discretization but not on h (for large enough problems). Thus, if the time step is chosen as a fraction of the stability limit, the theoretical execution time for a given problem size is proportional to $\sqrt{\rho(\tilde{D})}$.

7. Numerical experiments

In this section, we numerically verify and compare the methods. We evaluate the methods in terms of error convergence and theoretical execution time measured as the spectral radius of the undivided spatial operator (as outlined in Section 6).

7.1. Analytical solutions

To measure the error and convergence of the methods we use standing waves solutions derived using separation of variables. The form of the analytical solutions are given by

$$u(x,t) = T(t)X(x), \tag{75}$$

where

$$T(t) = \cos(\beta^2 \sqrt{\frac{a}{b}} t) \quad \text{and} \tag{76}$$

$$X(x) = A_1 \cosh(\beta x) + A_2 \cos(\beta x) + A_3 \sin(\beta x) + A_4 \sinh(\beta x). \tag{77}$$

The constants $A_{1,2,3,4}$ and β are found by imposing the boundary or interface conditions and solving the resulting non-linear system of equations numerically. For the multiblock problem, the solutions in each block are given by (75) with separate parameters.

To evaluate the boundary treatments homogeneous beams with clamped and free homogeneous boundary conditions are considered. For these problems we choose $b = a = 1$ and the domain $x \in [0, 1]$. The interface treatments are evaluated by considering a periodic domain $x \in [-1, 1]$ with a parameter discontinuity at $x = 0$ and $x = \pm 1$ (two interface couplings). The parameters are chosen to $a^{(1)} = 1$, $a^{(2)} = 4$ and $b^{(1)} = b^{(2)} = 1$. The solutions at $t = 0$ (initial data) are plotted in Fig. 2. In Appendix A the parameters $A_{1,2,3,4}$ and β for the homogeneous beam with clamped and free boundary conditions and parameters $A^{(1,2)}_{1,2,3,4}$ and $\beta^{(1,2)}$ for the piecewise homogeneous beam are presented.

The error is calculated as

$$\epsilon^{(m)} = \|u - v^{(m)}\|_h, \tag{78}$$

where u is the analytical solution, $v^{(m)}$ is the approximate solution with m grid points, and $\|\cdot\|_h$ is the discrete L^2-norm. The time step is chosen as the stability requirement divided by two. The errors are measured at $t = 1$.

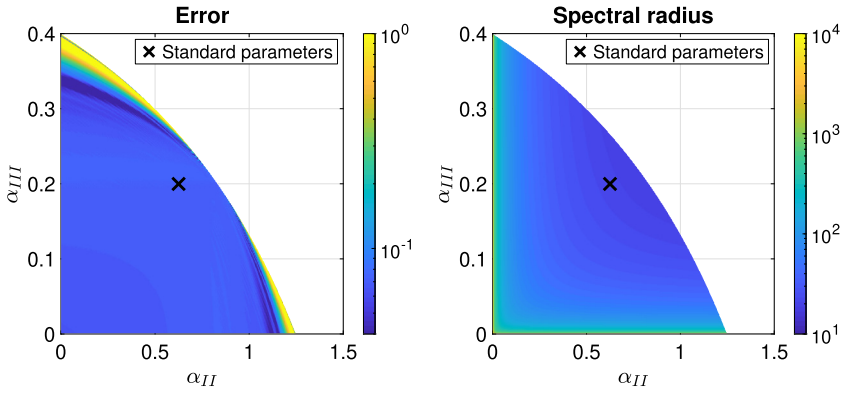

(a) 2nd order operators.

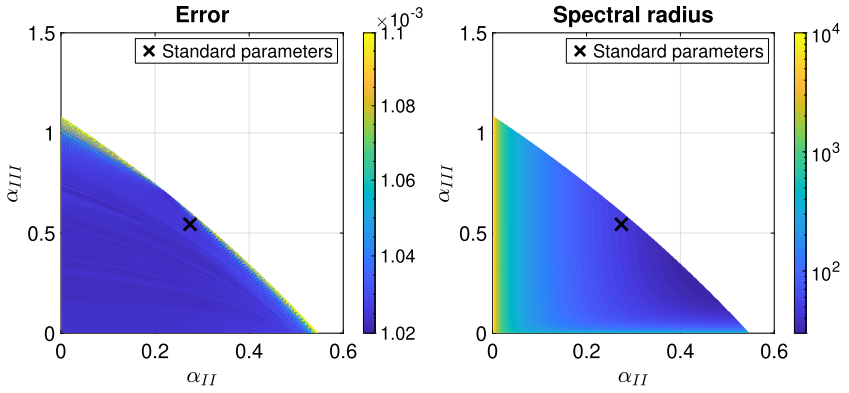

(b) 4th order operators.

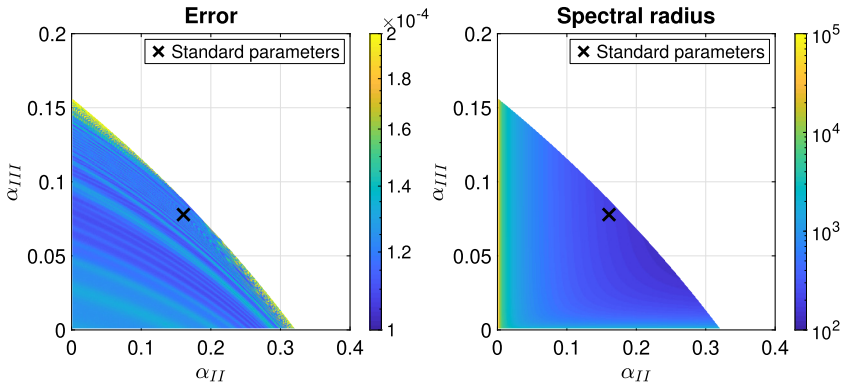

(c) 6th order operators.

Fig. 3. Error and undivided spectral radius with stable α_{II} and α_{III} for the 2nd, 4th, and 6th order SBP operators applied to homogeneous beam problem with clamped boundary conditions. The standard parameters are indicated. (For interpretation of the colors in the figure(s), the reader is referred to the web version of this article.)

7.2. Choice of α_{II} and α_{III} for SAT

When imposing clamped boundary conditions with SAT or interface conditions with only SAT one has to decide how to choose the parameters α_{II} and α_{III}, see Sections 4.3 and 5.3. In this section, we investigate the influence of these parameters on the error and spectral radius (theoretical execution time, see Section 6) for the homogeneous DBE with clamped boundary conditions.

In Fig. 3 the error and undivided spectral radius for stable choices of α_{II} and α_{III} are plotted for the 2nd, 4th, and 6th order operators with $m = 21$. For all orders the spectral radius is greatest for small $\alpha_{II,III}$. This is expected since it leads to SAT with a larger magnitude, and thus the boundary conditions are imposed more strongly.

Table 1
Standard α_{II} and α_{III} for the 2nd, 4th, and 6th order operators.

Parameter	2nd order	4th order	6th
α_{II}	0.625	0.274	0.161
α_{III}	0.200	0.544	0.078

Table 2
Spectral radius of undivided right-hand side matrix $\tilde{D}$ for a homogeneous beam with clamped and free boundary conditions imposed using SAT and projection.

BC	Method	2nd order	4th order	6th order
Clamped	SAT	22.4651	49.8208	202.8492
	Projection	16.0000	26.6666	34.1333
Free	SAT	16.0000	28.3942	84.0057
	Projection	16.0000	26.6666	34.1333

Table 3
Spectral radius of undivided right-hand side matrix $\tilde{D}$ for a piecewise homogeneous beam with interface conditions imposed using SAT, projection, and hybrid.

Method	2nd order	4th order	6th order
SAT	64.1945	106.6666	367.1694
Projection	64.0000	106.6666	136.5332
Hybrid	64.0000	106.6666	193.7828

As can be seen in the error plots of all orders, the smallest spectral radius leads to a relatively large error and, in some cases, the smallest error leads to the largest spectral radius. It is not clear whether or not an optimal choice exists. In this paper, we use the parameters derived in [16], given by the largest α_{II} and α_{III} such that

$$\begin{aligned} &\frac{N}{2} - h\alpha_{II}(d_{2;l}d_{2;l}^{\top} + d_{2;r}d_{2;r}^{\top}) \geq 0 \quad \text{and} \\ &\frac{N}{2} - h^3\alpha_{III}(d_{3;l}d_{3;l}^{\top} + d_{3;r}d_{3;r}^{\top}) \geq 0. \end{aligned} \tag{79}$$

These parameters, here referred to as *standard*, are determined numerically and presented in Table 1 and Fig. 3. Clearly, for this problem, the standard parameters are not optimal. However, we have found by extensive testing that this choice leads to a reliable balance between error and spectral radius. Furthermore, computing the standard parameters is cheap and problem independent. Performing a parameter sweep such as the one used to generate Fig. 3 is highly expensive and not feasible for individual problems. In the present study, we settle with using the standard parameters for the purpose of comparing SAT to projection. The question of optimal parameter choices is an interesting topic for future research.

7.3. Spectral radius

In this section, we present and compare the spectral radii of the spatial operators for the homogeneous and piecewise homogeneous beam problems.

In Table 2 the undivided spectral radii for the homogeneous beam problem with clamped and free boundary conditions imposed using SAT and projection are presented. The results show that the projection method leads to a smaller spectral radius, thus allowing for a larger time step, compared to SAT. Note also that the spectral radius with boundary conditions imposed using projection is independent of boundary conditions, whereas the clamped boundary conditions with SAT yield a significantly larger spectral radius compared to free boundary conditions with SAT.

In Table 3 the undivided spectral radii for the piecewise homogeneous beam problem with interface conditions imposed using SAT, projection, and the hybrid method are shown. For the 2nd and 4th order operators, the spectral radius is independent of the method. For the 6th order operators, the projection method yields the smallest spectral radius and SAT the largest.

7.4. Error convergence

In this section, we present accuracy and convergence results for the homogeneous and piecewise homogeneous beam problems. The theoretical rate of convergence for this problem is $\min(2p, r+4)$, where $2p$ is the internal stencil order and r is the boundary closure order [22]. For the 2nd, 4th, and 6th order SBP operators used here we have $p = 1, 2, 3$ and

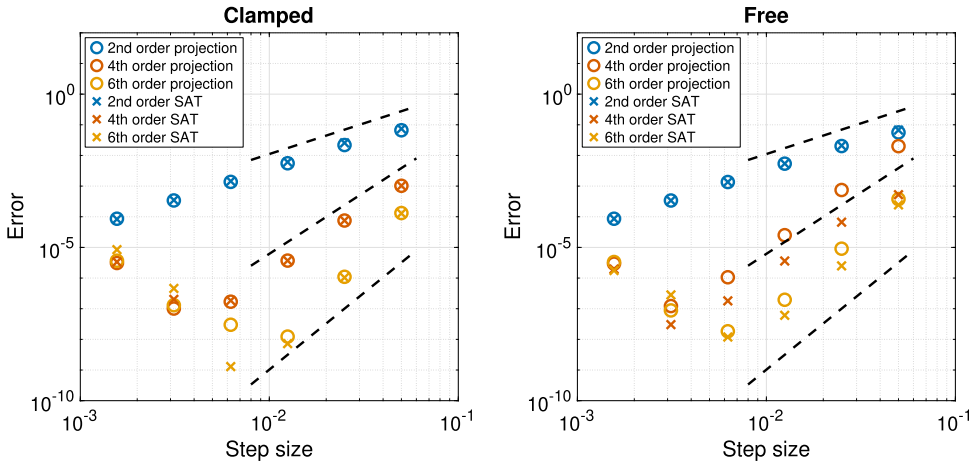

Fig. 4. Error as a function of step size for a homogeneous beam with clamped and free boundary conditions imposed using SAT and projection. Results with 2nd, 4th, and 6th order SBP operators are presented. The dashed lines indicate the theoretical convergence rates 2, 4, and 5.

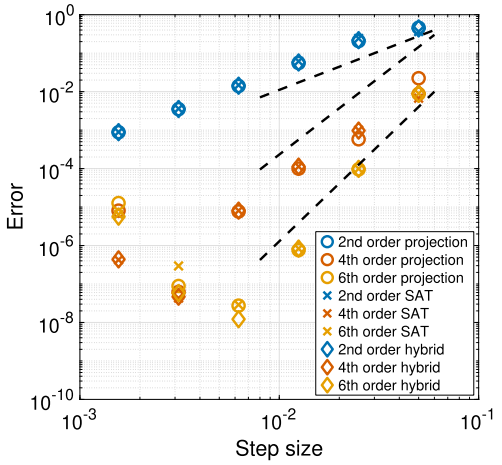

Fig. 5. Error as a function of step size for circular piecewise homogeneous beam imposed using SAT, projection and hybrid method. Results with 2nd, 4th, and 6th order SBP operators are presented. The dashed lines indicate the theoretical convergence rates 2, 4, and 5.

$r = -2, 0, 1$ (see [18] for more details). Thus, the theoretical convergence rates are 2, 4, and 5 for the 2nd, 4th, and 6th order SBP operators respectively.

In Fig. 4 the errors of the homogeneous beam problem with clamped and free boundary conditions imposed using SAT and projection are plotted for the 2nd, 4th, and 6th order operators. The plots indicate good agreement with the theoretical convergence expectations for large step sizes. The roundoff errors are dominant with the 4th and 6th order operators for approximately $h < 5 \cdot 10^{-3}$. The results show that the error with SAT and projection are comparable for clamped boundary conditions, and that SAT is slightly more accurate for free boundary conditions.

In Fig. 5 we compare the errors for the piecewise homogeneous beam with interface conditions imposed using SAT, projection, and the hybrid method. The results show that all three methods for imposing interface conditions are comparable in terms of error and that the expected convergence rates with all operators are obtained for large h.

8. Kirchoff-Love plate equation

To demonstrate that the methods can be extended to two-dimensional problems, we briefly consider the Kirchoff-Love plate equation, given by

$$bu_{tt} = -a\Delta^2 u = -a(u_{xxxx} + 2u_{xxyy} + u_{yyyy}), \quad x, y \in \Omega \tag{80}$$

with clamped boundary conditions, given by

$$u = \frac{\partial u}{\partial n} = 0, \quad x, y \in \partial\Omega. \tag{81}$$

Here $\Omega = [x_l, x_r] \times [y_l, y_r]$ defines a rectangular domain, $\partial\Omega$ denotes its boundary, and n is the outward pointing normal.

Multiplying (80) by u_t, integrating over Ω, and using integration by parts repeatedly lead to

$$\begin{aligned}\frac{d}{dt}E = -4a[[u_t u_{xy}]_{y_l}^{y_r}]_{x_l}^{x_r} &+ 2a\int_{y_l}^{y_r}[-u_t u_{xxx} + u_{tx}u_{xx} + 2u_{ty}u_{xy}]_{x_l}^{x_r}\,dy \\ &+ 2a\int_{x_l}^{x_r}[-u_t u_{yyy} + u_{ty}u_{yy} + 2u_{tx}u_{xy}]_{y_l}^{y_r}\,dx,\end{aligned} \tag{82}$$

where

$$E = b\|u_t\|^2 + a\|u_{xx}\|^2 + 2a\|u_{xy}\|^2 + a\|u_{yy}\|^2. \tag{83}$$

Imposing the boundary conditions (81) leads to energy conservation

$$\frac{d}{dt}E = 0. \tag{84}$$

We now place an interface at $x = 0$ (assuming $x_l < 0$ and $x_r > 0$) and let $a^{(1,2)}$ and $b^{(1,2)}$ denote the material parameters in the left and right blocks. Following the reasoning in Section 5, the PDE is split at the interface as follows:

$$\begin{aligned} b^{(1)}u_{tt}^{(1)} &= -a^{(1)}(u_{xxxx}^{(1)} + 2u_{xxyy}^{(1)} + u_{yyyy}^{(1)}), \quad x, y \in \Omega^{(1)}, \\ b^{(2)}u_{tt}^{(2)} &= -a^{(2)}(u_{xxxx}^{(2)} + 2u_{xxyy}^{(2)} + u_{yyyy}^{(2)}), \quad x, y \in \Omega^{(2)}, \end{aligned} \tag{85}$$

where $\Omega^{(1)} = [x_l, 0] \times [y_l, y_r]$ and $\Omega^{(2)} = [0, x_r] \times [y_l, y_r]$. Ignoring terms corresponding to outer boundaries, the energy equation becomes

$$\begin{aligned}\frac{d}{dt}E = \Big[&- 4[a^{(1)}u_t^{(1)}u_{xy}^{(1)} - a^{(2)}u_t^{(2)}u_{xy}^{(2)}]_{y_l}^{y_r} \\ &+ 2\int_{y_l}^{y_r} a^{(1)}(-u_t^{(1)}u_{xxx}^{(1)} + u_{tx}^{(1)}u_{xx}^{(1)} + 2u_{ty}^{(1)}u_{xy}^{(1)}) \\ &+ a^{(2)}(u_t^{(2)}u_{xxx}^{(2)} - u_{tx}^{(2)}u_{xx}^{(2)} - 2u_{ty}^{(2)}u_{xy}^{(2)})\,dy\Big]_{x=0}\end{aligned} \tag{86}$$

where

$$E = \sum_{i=1,2} b^{(i)}\|u_t^{(i)}\|^2 + a^{(i)}(\|u_{xx}^{(i)}\|^2 + 2\|u_{xy}^{(i)}\|^2 + \|u_{yy}^{(i)}\|^2). \tag{87}$$

If the interface conditions

$$\begin{aligned} u^{(1)} &= u^{(2)}, \\ a^{(1)}u_x^{(1)} &= a^{(2)}u_x^{(2)}, \\ u_{xx}^{(1)} &= u_{xx}^{(2)}, \\ a^{(1)}u_{xxx}^{(1)} &= a^{(2)}u_{xxx}^{(2)}, \end{aligned} \tag{88}$$

are satisfied at $x = 0$, the right-hand side of (86) is zero and the energy is conserved.

8.1. Spatial discretization

The PDE is discretized using SBP operators with the boundary and interface conditions imposed using a hybrid projection and SAT method. The one-dimensional SBP operators are extended to 2D using the following definitions:

$$\begin{aligned} D_{2x} &= D_2 \otimes I_m, & D_{2y} &= I_m \otimes D_2, \\ D_{4x} &= D_4 \otimes I_m, & D_{4y} &= I_m \otimes D_4, \\ e_W &= e_1 \otimes I_m, & d_{(1,2,3);W} &= d_{(1,2,3);l} \otimes I_m, \\ e_E &= e_m \otimes I_m, & d_{(1,2,3);E} &= d_{(1,2,3);r} \otimes I_m, \\ e_S &= I_m \otimes e_1, & d_{(1,2,3);S} &= I_m \otimes d_{(1,2,3);l}, \\ e_N &= I_m \otimes e_m, & d_{(1,2,3);N} &= I_m \otimes d_{(1,2,3);r}. \end{aligned} \tag{89}$$

We also have the two-dimensional inner product matrices

$$H_x = H \otimes I_m, \quad H_y = I_m \otimes H, \quad \text{and} \quad H_{xy} = H_x H_y = H \otimes H. \tag{90}$$

The global two-block inner product is given by

$$\hat{H} = \begin{bmatrix} H_{xy} & 0 \\ 0 & H_{xy} \end{bmatrix}. \tag{91}$$

Let $w = \begin{bmatrix} v^{(1)} \\ v^{(2)} \end{bmatrix}$ denote the global semi-discrete solution vector, where $v^{(1)}$ and $v^{(2)}$ are column-major ordered semi-discrete solution vectors in the left and right blocks, respectively. A consistent semi-discrete approximation of (85) using SBP-SAT-P is

$$(B \otimes I_{m^2}) w_{tt} = P(D + SAT_1 + SAT_2) P w, \tag{92}$$

where

$$P = I_{2m^2} - \hat{H}^{-1} L^\top (L \hat{H}^{-1} L)^{-1} L, \tag{93}$$

$$D = \begin{bmatrix} -a^{(1)}(D_{4x} + 2D_{2x}D_{2y} + D_{4y}) & 0 \\ 0 & -a^{(2)}(D_{4x} + 2D_{2x}D_{2y} + D_{4y}) \end{bmatrix}, \tag{94}$$

$$SAT_1 = \begin{bmatrix} \tau_1 a^{(1)} H_{xy}^{-1} e_E H d_{3;E}^\top & \tau_1 a^{(2)} H_{xy}^{-1} e_E H d_{3;W}^\top \\ \sigma_1 a^{(1)} H_{xy}^{-1} e_W H d_{3;E}^\top & \sigma_1 a^{(2)} H_{xy}^{-1} e_W H d_{3;W}^\top \end{bmatrix}, \tag{95}$$

and

$$SAT_2 = \begin{bmatrix} \tau_2 H_{xy}^{-1} d_{1;E} H d_{2;E}^\top & \tau_2 H_{xy}^{-1} d_{1;E} H d_{2;W}^\top \\ \sigma_2 H_{xy}^{-1} d_{1;W} H d_{2;E}^\top & \sigma_2 H_{xy}^{-1} d_{1;W} H d_{2;W}^\top \end{bmatrix}. \tag{96}$$

The penalty terms SAT_1 and SAT_2 impose the last two conditions in (88) weakly using the SAT method, where $\tau_{1,2}$ and $\sigma_{1,2}$ are scalars tuned for stability. The boundary conditions and remaining interface conditions are given by $Lw = 0$, where

$$L = \begin{bmatrix} L_{BC}^{(1)} & 0 \\ 0 & L_{BC}^{(2)} \\ & L_{IC} \end{bmatrix} \tag{97}$$

and

$$L_{BC}^{(1)} = \begin{bmatrix} e_W^\top \\ e_S^\top \\ e_N^\top \\ d_{1;W}^\top \\ d_{1;S}^\top \\ d_{1;N}^\top \end{bmatrix}, \quad L_{BC}^{(2)} = \begin{bmatrix} e_E^\top \\ e_S^\top \\ e_N^\top \\ d_{1;E}^\top \\ d_{1;S}^\top \\ d_{1;N}^\top \end{bmatrix}, \quad L_{IC} = \begin{bmatrix} e_E^\top & -e_W^\top \\ a^{(1)} d_{1;E}^\top & a^{(2)} d_{1;W}^\top \end{bmatrix}. \tag{98}$$

Lemma 8. *The system (92) is a stable approximation of the piecewise continuous Kirchoff-Love plate equation (85) if D_2 and D_4 are SBP operators built on the same norm, and if*

$$\tau_1 = 1 - \sigma_1 \quad \textit{and} \quad \tau_2 = \sigma_2 \frac{a^{(1)}}{a^{(2)}} - a^{(1)}. \tag{99}$$

Proof. Multiplying (92) by $w_t^\top \hat{H}$ and using Definition 1 lead to

$$\frac{d}{dt} E = a^{(1)} BT^{(1)} + a^{(2)} BT^{(2)} + IT, \tag{100}$$

where the boundary terms are

$$\begin{aligned} BT^{(1)} = &-2(e_W^\top \tilde{v}_t^{(1)})^\top H d_{3;W}^\top \tilde{v}^{(1)} - 2(d_{1;W}^\top \tilde{v}_t^{(1)})^\top H d_{2;W}^\top \tilde{v}^{(1)} + 4(e_W^\top \tilde{v}_t^{(1)})^\top M d_{1;W}^\top \tilde{v}^{(1)} \\ &- 2(e_S^\top \tilde{v}_t^{(1)})^\top H d_{3;S}^\top \tilde{v}^{(1)} - 2(d_{1;S}^\top \tilde{v}_t^{(1)})^\top H d_{2;S}^\top \tilde{v}^{(1)} + 4(e_S^\top \tilde{v}_t^{(1)})^\top M d_{1;S}^\top \tilde{v}^{(1)} \\ &- 2(e_N^\top \tilde{v}_t^{(1)})^\top H d_{3;N}^\top \tilde{v}^{(1)} + 2(d_{1;N}^\top \tilde{v}_t^{(1)})^\top H d_{2;N}^\top \tilde{v}^{(1)} + 4(e_N^\top \tilde{v}_t^{(1)})^\top M d_{1;N}^\top \tilde{v}^{(1)} \\ &- 4(e_l^\top e_S^\top \tilde{v}_t^{(1)})(d_{1;l}^\top d_{1;S}^\top \tilde{v}^{(1)}) - 4(e_l^\top e_N^\top \tilde{v}_t^{(1)})(d_{1;l}^\top d_{1;N}^\top \tilde{v}^{(1)}) \\ &- 4(e_r^\top e_S^\top \tilde{v}_t^{(1)})(d_{1;r}^\top d_{1;S}^\top \tilde{v}^{(1)}) - 4(e_r^\top e_N^\top \tilde{v}_t^{(1)})(d_{1;r}^\top d_{1;N}^\top \tilde{v}^{(1)}), \end{aligned} \tag{101}$$

and

$$\begin{aligned} BT^{(2)} = &-2(e_E^\top \tilde{v}_t^{(2)})^\top H d_{3;E}^\top \tilde{v}^{(2)} + 2(d_{1;E}^\top \tilde{v}_t^{(2)})^\top H d_{2;E}^\top \tilde{v}^{(2)} + 4(e_E^\top \tilde{v}_t^{(2)})^\top M d_{1;E}^\top \tilde{v}^{(2)} \\ &- 2(e_S^\top \tilde{v}_t^{(2)})^\top H d_{3;S}^\top \tilde{v}^{(2)} - 2(d_{1;S}^\top \tilde{v}_t^{(2)})^\top H d_{2;S}^\top \tilde{v}^{(2)} + 4(e_S^\top \tilde{v}_t^{(2)})^\top M d_{1;S}^\top \tilde{v}^{(2)} \\ &- 2(e_N^\top \tilde{v}_t^{(2)})^\top H d_{3;N}^\top \tilde{v}^{(2)} + 2(d_{1;N}^\top \tilde{v}_t^{(2)})^\top H d_{2;N}^\top \tilde{v}^{(2)} + 4(e_N^\top \tilde{v}_t^{(2)})^\top M d_{1;N}^\top \tilde{v}^{(2)} \\ &- 4(e_l^\top e_S^\top \tilde{v}_t^{(2)})(d_{1;l}^\top d_{1;S}^\top \tilde{v}^{(2)}) - 4(e_l^\top e_N^\top \tilde{v}_t^{(2)})(d_{1;l}^\top d_{1;N}^\top \tilde{v}^{(2)}) \\ &- 4(e_r^\top e_S^\top \tilde{v}_t^{(2)})(d_{1;r}^\top d_{1;S}^\top \tilde{v}^{(2)}) - 4(e_r^\top e_N^\top \tilde{v}_t^{(2)})(d_{1;r}^\top d_{1;N}^\top \tilde{v}^{(2)}), \end{aligned} \tag{102}$$

the interface terms are

$$\begin{aligned} IT = &-2a^{(1)}(e_E^\top \tilde{v}_t^{(1)})^\top H d_{3;E}^\top \tilde{v}^{(1)} - 2a^{(2)}(e_W^\top \tilde{v}_t^{(2)})^\top H d_{3;W}^\top \tilde{v}^{(2)} \\ &+ 2a^{(1)}(d_{1;E}^\top \tilde{v}_t^{(1)})^\top H d_{2;E}^\top \tilde{v}^{(1)} - 2a^{(2)}(d_{1;W}^\top \tilde{v}_t^{(2)})^\top H d_{2;W}^\top \tilde{v}^{(2)} \\ &+ 4a^{(1)}(e_E^\top \tilde{v}_t^{(1)})^\top M d_{1;E}^\top \tilde{v}^{(1)} + 4a^{(2)}(e_W^\top \tilde{v}_t^{(2)})^\top M d_{1;W}^\top \tilde{v}^{(2)} \\ &+ 2\tau_1(e_E^\top \tilde{v}_t^{(1)})^\top H(a^{(1)} d_{3;E}^\top \tilde{v}^{(1)} + a^{(2)} d_{3;W}^\top \tilde{v}^{(2)}) \\ &+ 2\tau_2(d_{1;E}^\top \tilde{v}_t^{(1)})^\top H(d_{2;E}^\top \tilde{v}^{(1)} + d_{2;W}^\top \tilde{v}^{(2)}) \\ &+ 2\sigma_1(e_W^\top \tilde{v}_t^{(2)})^\top H(a^{(2)} d_{3;W}^\top \tilde{v}^{(2)} + a^{(1)} d_{3;E}^\top \tilde{v}^{(1)}) \\ &+ 2\sigma_2(d_{1;W}^\top \tilde{v}_t^{(2)})^\top H(d_{2;W}^\top \tilde{v}^{(2)} + d_{2;E}^\top \tilde{v}^{(1)}), \end{aligned} \tag{103}$$

and the energy is given by

$$E = \sum_{i=1,2} b^{(i)}(v_t^{(i)})^\top (H \otimes H) v_t^{(i)} + a^{(i)}(\tilde{v}^{(i)})^\top ((N \otimes H) + 2(M \otimes M) + (H \otimes N))\tilde{v}^{(i)}. \tag{104}$$

Here $\tilde{w} = \begin{bmatrix} \tilde{v}^{(1)} \\ \tilde{v}^{(2)} \end{bmatrix} = Pw$ denotes the projected solution vector. Since $L\tilde{w} = LPw = 0$, we have $L_{BC}^{(1)}\tilde{v}^{(1)} = 0$ and $L_{BC}^{(2)}\tilde{v}^{(2)} = 0$. From this it immediately follows that $BT^{(1)} = BT^{(2)} = 0$. Additionally, since $L_{IC}\tilde{w} = 0$, we have

$$\begin{aligned} e_E^\top \tilde{v}^{(1)} &= e_W^\top \tilde{v}^{(2)}, \\ a^{(1)} d_{1;E}^\top \tilde{v}^{(1)} &= -a^{(2)} d_{1;W}^\top \tilde{v}^{(2)}. \end{aligned} \tag{105}$$

Substituting into (103) gives

$$\begin{aligned} IT = &2(-1 + \tau_1 + \sigma_1)(e_E^\top \tilde{v}_t^{(1)})^\top H(a^{(1)} d_{3;E}^\top \tilde{v}^{(1)} + a^{(2)} d_{3;W}^\top \tilde{v}^{(2)}) \\ &+ 2(a^{(1)} + \tau_2 - \sigma_2 \frac{a^{(1)}}{a^{(2)}})(d_{1;E}^\top \tilde{v}_t^{(1)})^\top H(d_{2;E}^\top \tilde{v}^{(1)} + d_{2;W}^\top \tilde{v}^{(2)}) \end{aligned} \tag{106}$$

Choosing

$$\tau_1 = 1 - \sigma_1 \quad \text{and} \quad \tau_2 = \sigma_2 \frac{a^{(1)}}{a^{(2)}} - a^{(1)}, \tag{107}$$

lead to energy conservation,

$$\frac{d}{dt} E = 0, \tag{108}$$

and thus the scheme is stable. □

To make the penalties on both sides of the interface equal in magnitude, we choose

$$\tau_1 = 0.5, \quad \sigma_1 = 0.5, \quad \tau_2 = \frac{-a^{(1)}a^{(2)}}{a^{(1)} + a^{(2)}}, \quad \text{and} \quad \sigma_2 = \frac{a^{(1)}a^{(2)}}{a^{(1)} + a^{(2)}}. \tag{109}$$

8.2. Convergence study

To verify the accuracy of the discretization we perform a convergence study against a reference solution on the domain $\Omega = [-1, 1] \times [0, 1]$ with an interface at $x = 0$. The PDE is initiated with a Gaussian pulse in the right block and simulated until $t = 0.03$. The material parameters are given by $b^{(1,2)} = a^{(1)} = 1$ and $a^{(2)} = 4$. The system of ODE:s is integrated in time using the explicit scheme described in Section 6.

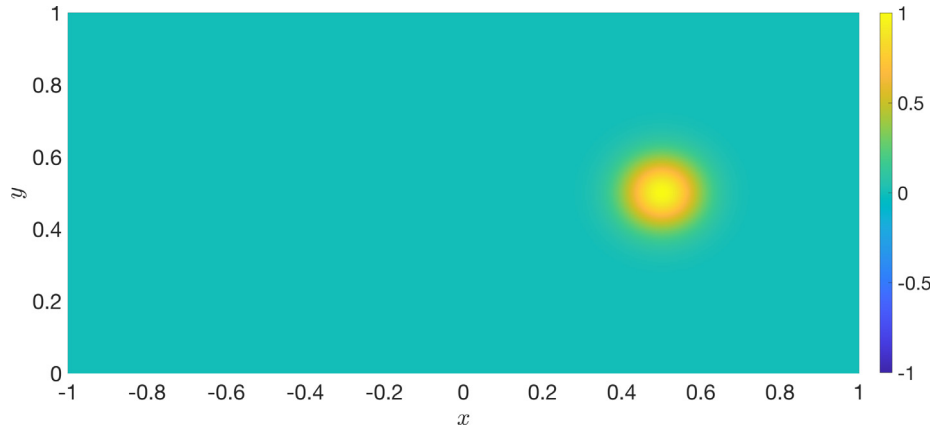

(a) Initial data.

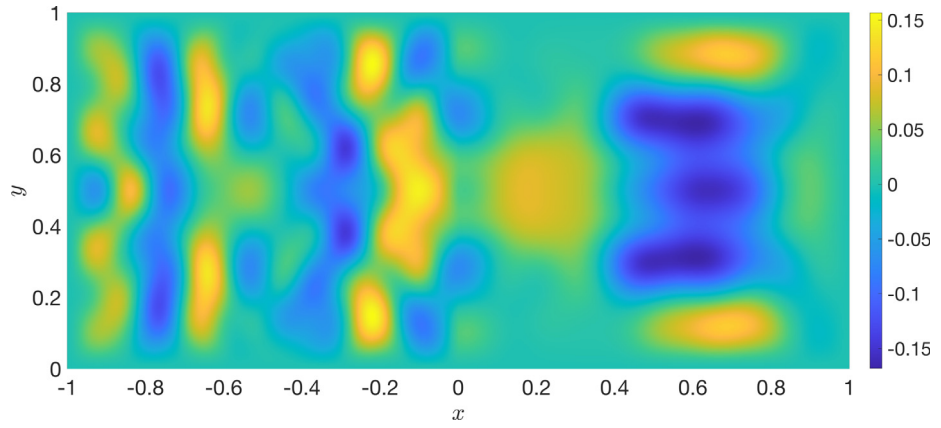

(b) Reference solution at $t = 0.03$.

Fig. 6. Initial and reference solution of the Kirchoff-Love plate equation with a parameter discontinuity at $x = 0$. Obtained using the 6th order operators with 401×401 grid points.

Table 4
Error and convergence results for the piecewise continuous Kirchoff-Love plate equation with m grid points in each dimension and block and the 4th and 6th order SBP operators.

m	Error 4th	Convergence 4th	Error 6th	Convergence 6th
21	-1.31	-	-1.45	-
41	-1.94	-2.16	-2.22	-2.64
51	-2.21	-2.83	-2.70	-5.12
81	-3.09	-4.38	-3.83	-5.61
101	-3.50	-4.32	-4.34	-5.30

In Fig. 6 the initial data and reference solution at $t = 0.03$ are plotted. The reference solution is obtained using the 6th order SBP operators and 401×401 grid points in each block. In Table 4 the error and convergence results measured against the reference solution in the $\hat{H}$-norm for the 4th and 6th order operators are presented. With both sets of operators, we obtain the expected theoretical rates of convergence, 4 and 5.

9. Conclusions

In this paper, we have studied boundary treatments for the dynamic beam equation (DBE) using summation-by-parts finite differences (SBP-FD). We have compared the simultaneous approximation term (SAT) method to the projection method in terms of accuracy and efficiency for the DBE with clamped and free boundary conditions. We have also studied the DBE with piecewise constant parameters, where the discontinuities necessitate the use of internal boundaries. Novel SAT and projection methods for imposing the interface conditions are derived. Additionally, we present a novel hybrid method combining SAT and projection for interface conditions. The accuracy and efficiency of the methods are compared numerically. We also demonstrate that the methods can be extended to two spatial dimensions by deriving a stable SBP-SAT-P

discretization of the piecewise homogeneous dynamic Kirchoff-Love plate equation. The theoretically expected convergence behavior is shown using a reference solution.

Numerical experiments with specific SBP-FD operators show that the SAT method can be more accurate than the projection method for free boundary conditions. Otherwise, all methods considered are comparable in terms of accuracy. The projection method is found to yield the smallest spectral radius for all problems considered, thus leading to the least restrictive time step requirement for explicit time integration methods.

Awaiting further theoretical developments all methods are roughly equal and the choice between them is largely a matter of taste. However, we emphasize the difference between SAT and projection when proving stability of SBP discretizations. With the projection method the proofs closely mimic the continuous counterparts. One may argue that, for the problems considered here, the derivation of a semi-discrete energy estimate is redundant since it directly follows from the continuous proof if SBP-FD operators are used together with projection. With the SAT method the proofs are more involved, in particular for clamped boundary conditions and interface conditions since these involve the decomposition of the fourth derivative operator and tuning of multiple parameters. The hybrid method for interface conditions avoids these problems but, as the numerical experiments show, it is not more accurate nor more efficient than the projection method.

CRediT authorship contribution statement

Gustav Eriksson: Conceptualization, Investigation, Software, Writing – original draft, Writing – review & editing. **Jonatan Werpers:** Conceptualization, Investigation, Software, Writing – review & editing. **David Niemelä:** Investigation, Software. **Niklas Wik:** Investigation, Software. **Valter Zethrin:** Investigation, Software. **Ken Mattsson:** Conceptualization, Supervision, Writing – review & editing.

Declaration of competing interest

The authors declare that they have no known competing financial interests or personal relationships that could have appeared to influence the work reported in this paper.

Data availability

Data will be made available on request.

Acknowledgements

Ken Mattsson is partially supported by the Swedish Research Council (grant 2017-04626), and FORMAS (grant 2018-00925).

Appendix A. Parameters of analytical solutions

See Tables A.5 and A.6.

Table A.5
Parameters for analytical solutions (75) of a homogeneous beam with clamped and free boundary conditions.

	Clamped	Free
β	4.730040744862704	4.730040744862704
A_1	1.0	1.0
A_2	−1.0	1.0
A_3	−0.982502214576238	−0.982502214576238
A_4	0.982502214576238	−0.982502214576238

References

[1] J.Y. Lee, W. Jeon, Exact solution of Euler-Bernoulli equation for acoustic black holes via generalized hypergeometric differential equation, J. Sound Vib. 452 (2019) 191–204, https://doi.org/10.1016/j.jsv.2019.02.016.

[2] P.J. Gonçalves, M.J. Brennan, S.J. Elliott, Numerical evaluation of high-order modes of vibration in uniform Euler-Bernoulli beams, J. Sound Vib. 301 (3–5) (2007) 1035–1039, https://doi.org/10.1016/j.jsv.2006.10.012.

[3] G. Štimac Rončević, B. Rončević, A. Skoblar, R. Žigulić, Closed form solutions for frequency equation and mode shapes of elastically supported Euler-Bernoulli beams, J. Sound Vib. 457 (2019) 118–138, https://doi.org/10.1016/j.jsv.2019.04.036.

[4] H. Yu, Y. Yang, Y. Yuan, Analytical solution for a finite Euler–Bernoulli beam with single discontinuity in section under arbitrary dynamic loads, Appl. Math. Model. 60 (2018) 571–580, https://doi.org/10.1016/j.apm.2018.03.046.

[5] R. Ansari, K. Hosseini, A. Darvizeh, B. Daneshian, A sixth-order compact finite difference method for non-classical vibration analysis of nanobeams including surface stress effects, Appl. Math. Comput. 219 (10) (2013) 4977–4991, https://doi.org/10.1016/j.amc.2012.11.045.

Table A.6
Parameters for analytical solutions (75) of a piecewise homogeneous beam coupled as a ring.

	Interface
$\beta^{(1)}$	−7.5615808319278868
$A_1^{(1)}$	0.6114706121627287
$A_2^{(1)}$	−1.5276874719563509
$A_3^{(1)}$	2.0552837081134849
$A_4^{(1)}$	−0.6121069366992447
$\beta^{(2)}$	−5.3468450827464249
$A_1^{(2)}$	0.0766810911329587
$A_2^{(2)}$	−0.9928979509265810
$A_3^{(2)}$	1.9635450880282364
$A_4^{(2)}$	0.0774150750075980

[6] S. De Rango, D.W. Zingg, Higher-order spatial discretization for turbulent aerodynamic computations, AIAA J. 39 (7) (2001) 1296–1304, https://doi.org/10.2514/2.1472.
[7] J.S. Hesthaven, A stable penalty method for the compressible Navier-Stokes equations: II. One-dimensional domain decomposition schemes, SIAM J. Sci. Comput. 18 (3) (1997), https://doi.org/10.1137/S1064827594276540.
[8] A. Bayliss, K.E. Jordan, B.J. LeMesurier, E. Turkel, A fourth-order accurate finite-difference scheme for the computation of elastic waves, Bull. Seismol. Soc. Am. 76 (4) (1986) 1115–1132.
[9] S. Abarbanel, A. Ditkowski, Asymptotically stable fourth-order accurate schemes for the diffusion equation on complex shapes, J. Comput. Phys. 133 (2) (1997) 279–288, https://doi.org/10.1006/jcph.1997.5653.
[10] S.K. Lele, Compact finite difference schemes with spectral-like resolution, J. Comput. Phys. 103 (1) (1992) 16–42, https://doi.org/10.1016/0021-9991(92)90324-R.
[11] J.E. Hicken, Output error estimation for summation-by-parts finite-difference schemes, J. Comput. Phys. 231 (9) (2012) 3828–3848, https://doi.org/10.1016/j.jcp.2012.01.031.
[12] K. Mattsson, J. Nordström, High order finite difference methods for wave propagation in discontinuous media, J. Comput. Phys. 220 (1) (2006) 249–269, https://doi.org/10.1016/j.jcp.2006.05.007.
[13] K. Mattsson, P. Olsson, An improved projection method, J. Comput. Phys. 372 (June 2018) 349–372, https://doi.org/10.1016/j.jcp.2018.06.030.
[14] M. Almquist, S. Wang, J. Werpers, Order-preserving interpolation for summation-by-parts operators at nonconforming grid interfaces, SIAM J. Sci. Comput. 41 (2) (2019), https://doi.org/10.1137/18M1191609.
[15] K. Mattsson, O. O'Reilly, Compatible diagonal-norm staggered and upwind SBP operators, J. Comput. Phys. 352 (2018) 52–75, https://doi.org/10.1016/j.jcp.2017.09.044.
[16] K. Mattsson, V. Stiernström, High-fidelity numerical simulation of the dynamic beam equation, J. Comput. Phys. 286 (2015) 194–213, https://doi.org/10.1016/j.jcp.2015.01.038.
[17] K. Mattsson, J. Werpers, High-fidelity numerical simulation of solitons in the nerve axon, J. Comput. Phys. 305 (2016) 793–816, https://doi.org/10.1016/j.jcp.2015.11.007.
[18] K. Mattsson, Diagonal-norm summation by parts operators for finite difference approximations of third and fourth derivatives, J. Comput. Phys. 274 (2014) 432–454, https://doi.org/10.1016/j.jcp.2014.06.027.
[19] K. Mattsson, F. Ham, G. Iaccarino, Stable and accurate wave-propagation in discontinuous media, J. Comput. Phys. 227 (19) (2008) 8753–8767, https://doi.org/10.1016/j.jcp.2008.06.023.
[20] P. Olsson, Summation by parts, projections, and stability. I, Math. Comput. 64 (211) (1995) 1035, https://doi.org/10.1090/s0025-5718-1995-1297474-x.
[21] P. Olsson, Summation by parts, projections, and stability. II, Math. Comput. 64 (212) (1995) 1473–1493, https://doi.org/10.1090/s0025-5718-1995-1308459-9.
[22] M. Svärd, J. Nordström, On the convergence rates of energy-stable finite-difference schemes, J. Comput. Phys. 397 (2019) 108819, https://doi.org/10.1016/j.jcp.2019.07.018.